Supporting Information:

Supplemental Material for "Kinetics-based Computational Catalyst Design Strategy for the Oxygen Evolution Reaction on Transition Metal Oxide Surfaces"

Craig P. Plaisance,*,†,‡ Simeon D. Beinlich,† and Karsten Reuter†

†*Chair for Theoretical Chemistry and Catalysis Research Center, Technische Universität München, Lichtenbergstr. 4, D-85747 Garching, Germany*

‡*Present Address: Cain Department of Chemical Engineering, Louisiana State University, Baton Rouge, LA 70803, USA*

E-mail: craig.plaisance@tum.de

Technical Details of the DFT Calculations

All electronic structure calculations were performed using spin-polarized density functional theory (DFT) as implemented in the Vienna Ab-initio Simulation Package (VASP).[S1] To allow for a decent accuracy at affordable computational cost the exchange-correlation energy was calculated at the generalized gradient approximation (GGA) level using the revised Perdew-Burke-Ernzerhof (RPBE) functional.[S2] The electron density was converged using the Pulay-mixing scheme with a mixing fraction of 0.1 for the total charge density and 0.4 for the magnetization density. The wave functions were constructed in a plane wave basis up to an energy cutoff of 400 eV, with the projector augmented wave (PAW) method used to describe the higher energy features. For the determination of the Kohn-Sham orbital populations, an error function distribution was used with a width of 0.2 eV on the (311) surface and 0.02 eV on the (110) surfaces. The Brillioun zone was sampled at only the Γ-point on the (311) surface and using a $2 \times 1 \times 1$ Γ-centered k-point mesh for the (110)-A and (110)-B surfaces.

A crucial issue when using GGA functionals for systems with localized 3d electrons like Co_3O_4 is to correct for the over-delocalization of these electrons caused by the spurious self-interaction present in these functionals.[S3] As in our previous work,[S4,S5] we corrected for this using the GGA+U method introduced by Anisimov and coworkers.[S6–S8] For Cr, Mn, Fe, Co, and Ni, we used the values of the U parameter determined in ref S9 using a self-consistent linear-response approach we developed previously.[S4] For V, we calculated a value of 3.89 eV.

For location minimum energy structures, the conjugate gradient algorithm was used with a convergence criterion of 0.05 eV/Å for the force on each atom. To locate transition states corresponding to saddle points, a nudged elastic band (NEB)[S10,S11] calculation was first performed with a convergence criterion of 0.3 eV/Å for the force on each atom. The NEB contained 6 images if a stable hydroxyl intermediate state was found and 10 images otherwise. By interpolating along the resulting reaction trajectory, an initial guess for the transition state was identified which was then optimized further using the dimer method[S12] until the

force on each atom was converged within 0.05 eV/Å. In a few cases, the transition state was not located at a saddle point but at a crossing between the potential energy surfaces of two electronic states. In these cases, we used a method for locating such intersystem crossings that we implemented in VASP. Details of this method are given in the section Method for Locating Intersystem Crossings. These calculations were also converged to atomic forces of 0.05 eV/Å. All structures found using the dimer method were verified to be true transition states by displacing the structure 0.1 Å in both directions along the dimer mode and performing a geometry optimization on each one to ensure that they converged to the correct reactant (or intermediate) and product structures.

Method for Locating Intersystem Crossings

The method we implemented in VASP for locating an intersystem crossing between the potential energy surfaces of two electronic states is adapted from the method of Bearpark et al. for locating a conical intersection.[S13] The only difference is that we neglect coupling between the two states by the Hamiltonian, as this is outside the context of the Kohn-Sham formalism. This method is implemented in VASP by running calculations of two images (labeled 1 and 2) in parallel that have the same geometric structure but different electronic structures. Because the two images have different electronic structures, the forces on the atoms in each one will be different. We define the $3N$ dimensional (N is the number of atoms in the system) reaction coordinate $\mathbf{g}$ as the normalized difference in these force vectors $\mathbf{F}_1$ and $\mathbf{F}_2$,

$$\mathbf{g} = \frac{\mathbf{F}_1 - \mathbf{F}_2}{\|\mathbf{F}_1 - \mathbf{F}_2\|} \quad . \tag{S1}$$

We then project out the force along this direction from either of the two images (the result is independent of which image we use) and add a force back along this direction that is

proportional to the difference between the energies E_1 and E_2 of the two electronic states,

$$\mathbf{F} = \mathbf{F}_2 - (\mathbf{F}_2 \cdot \mathbf{g})\mathbf{g} + \alpha(E_1 - E_2)\mathbf{g} \quad . \tag{S2}$$

The resulting force vector $\mathbf{F}$ is used with a conjugate gradient algorithm to locate the inter-system crossing. The parameter α is used to adjust the weight of the force along the reaction coordinate and was always set to a value of $10\,\text{Å}^{-1}$.

Method for Constraining Atomic Magnetic Moments

An additional challenge associated with systems having localized 3d electrons is that the electronic structure can often converge to several different local minima, typically associated with different spin states of each transition metal atom.[S14] In order to force the system to converge to a particular electronic state, we found it necessary to first run a calculation in which the magnetic moment on each transition metal atom is constrained to a certain value, and then use the resulting geometry and electronic structure as an initial guess to an unconstrained calculation. The magnetic moments were constrained using a method we implemented in VASP that assigns a penalty function to the Kohn-Sham energy functional of the form

$$E_{\text{c.m.}} = \frac{1}{2}\lambda \sum_I (M_I - M_I^0)^2 \quad , \tag{S3}$$

where M_I^0 is the constrained value of the magnetic moment M_I on atom I. The magnetic moment on each atom I is calculated by defining a projection operator P_I onto the subspace of 3d orbitals on this atom. These projection operator are the same as the projection operators used to define the 3d subspaces within the GGA+U method implemented in VASP (c.f. ref S15). A pseudo version of these projection operators is defined according to[S15]

$$\tilde{P}_I = \sum_{i,j \in I} |\tilde{p}_i\rangle \, \langle \phi_i | P_I | \phi_j \rangle \, \langle \tilde{p}_j | \quad . \tag{S4}$$

The magnetic moment on at I is then defined as

$$M_I = n_I^{\uparrow} - n_I^{\downarrow} \quad , \tag{S5}$$

where n_I^{σ} is the population of the spin-σ 3d subspace on atom I calculated using the pseudo Kohn-Sham orbitals $\tilde{\psi}_n^{\sigma}$ with occupancies f_n^{σ}

$$n_I^{\sigma} = \sum_n f_n^{\sigma} \langle \tilde{\psi}_n^{\sigma} | \tilde{P}_I | \tilde{\psi}_n^{\sigma} \rangle \quad . \tag{S6}$$

Finally, taking the variations of the energy penalty function in eq (S3) with respect to the pseudo Kohn-Sham orbitals leads to a constraining potential $V_{\text{c.m.}}$ that can be added to the Kohn-Sham potential to force the magnetic moments towards the constrained values,

$$V_{\text{c.m.}} = \lambda \sum_I (M_I - M_I^0) \tilde{P}^I \quad , \tag{S7}$$

where λ is an adjustable strength for the penalty function. In practice, λ was set to 1 eV, or to higher values in cases where the system still did not converge to the correct electronic state.

Procedure for Checking the Converged Electronic State

The electronic structures were checked for all calculations to ensure that all the 3d metal centers converged to the correct oxidation state and spin state. Table S1 shows the numbers of spin-up and spin-down 3d electrons on each metal corresponding to a given oxidation and spin state. Ni and Co exist in low-spin configurations while Fe and Mn exist in high-spin configurations. The high- and low-spin states are equivalent for Cr and V.

The number of 3d electrons of each spin on an atom was computed by counting the number of eigenvalues of the 3d orbital population matrices for that atom that were larger

than a threshold of 0.9. The assignment of electrons was considered to be unambiguous as long as all eigenvalues were above 0.9 or below 0.8. In some cases, there were eigenvalues between 0.8 and 0.9, making assignment of oxidation and spin states ambiguous. This procedure was used in our previous work[S4,S5] and is similar to a method proposed by Sit et al.[S16] The orbital population matrices on each atom were determined using the quasiatomic orbital method of Qian et al.[S17] which we implemented in VASP. Details of this approach are also given in our previous work.[S4,S5,S9]

Table S1: Number of spin-up and spin-down 3d electrons ($n_\uparrow/n_\downarrow$) for different oxidation and spin states (HS = high-spin, LS = low-spin) of the metal cations

		3+	4+	5+
Ni	LS	4/3	3/3	
Co	LS	3/3	3/2	3/1
Fe	HS	5/0	4/0	3/0
Mn	HS	4/0	3/0	2/0
Cr		3/0	2/0	1/0
V		2/0	1/0	0/0

Calculation of Free Energy Differences

reproduced and modified from ref S4

To determine the free energies of the different intermediates in the catalytic cycle, we use an approach similar to that of Rossmeisl, Nørskov, and coworkers in which the free energy of a proton and electron is determined by use of a reference reaction.[S18,S19] The most commonly used reference reaction is the hydrogen evolution reaction whereby the proton and electron are in equilibrium with H_2 gas at 1 bar, which is referred to as the computational hydrogen electrode. A more convenient choice for this study is to use the OER itself as the reference reaction so that the proton and electron are in equilibrium with O_2 at 1 bar and liquid water

$$2\,H_2O \rightleftharpoons O_2 + 4\,H^+ + 4\,e^- \quad . \qquad \{S1\}$$

At the potential where this reaction is in equilibrium ($\eta = 0$), the free energy of the proton and electron is equal to

$$G^\circ(\mathrm{H^+ + e^-}) = \frac{1}{2}G^\circ(\mathrm{H_2O}) - \frac{1}{4}G^\circ(\mathrm{O_2}) \quad . \tag{S8}$$

Due to the poor description of the O_2 molecule in DFT,[S19,S20] we use H_2 gas as the reference along with the experimental free energy of the OER, which is 4.92 eV under standard conditions so that

$$G^\circ(\mathrm{H^+ + e^-}) = \frac{1}{2}G^\circ(\mathrm{H_2}) + 1.23\,\mathrm{eV} \quad . \tag{S9}$$

When the overpotential is non-zero, the free energy of the proton and electron is simply increased by the overpotential η multiplied by the elementary charge

$$G(\mathrm{H^+ + e^-}) = G^\circ(\mathrm{H^+ + e^-}) + e\eta \quad . \tag{S10}$$

Since we only consider neutral systems in this study, it is not required to know the free energies of the proton and electron separately. Finally, since the elementary steps of the OER are written under alkaline conditions in the manuscript, we require the equality

$$G(\mathrm{e^-}) + G(\mathrm{H_2O}) - G(\mathrm{OH^-}) = G(\mathrm{H^+ + e^-}) \quad . \tag{S11}$$

This equality exists because self-ionization of water is an equilibrated process.

The other species for which a reference free energy is needed is liquid water. To get this value, we use the energy of water in the hexagonal ice structure at 0 K calculated by the same computational methods used throughout this study. The unit cell parameters used for this calculation (after relaxation) were $a = 7.82$ Å and $c = 8.63$ Å and the cell contained 8 water molecules. The results of this calculation give a cohesive energy of 0.50 eV per H_2O. Using the cohesive energy of ice at 0 K rather than the experimental free energy of vaporization of

water at standard conditions is reasonable because we do not include thermal effects in any of the other calculations in this work.

Derivation of the Rate Expression in Equation (1)

When the non-electrochemical water addition step is rate limiting, the turnover frequency (TOF) of a site is given by

$$\mathrm{TOF} = k_3 P_\mathrm{R} \quad , \tag{S12}$$

where k_3 is the intrinsic rate constant for non-electrochemical water addition and P_R is the probability of the site existing in the reactant state from which this reaction proceeds. This probability is given by the Boltzmann distribution,

$$P_\mathrm{R} = \frac{\exp\left(-\frac{G_\mathrm{R}}{k_\mathrm{B}T}\right)}{\sum_i \exp\left(-\frac{G_i}{k_\mathrm{B}T}\right)} \quad , \tag{S13}$$

where G_R is the free energy of the reactant state and the sum in the denominator runs over all possible states of the site (including the reactant state) with free energies G_i.

In our simplified kinetic model, we assume that the site can exist four possible states, differing by the oxidation state of the $(\mathrm{M-O})_a$ and $(\mathrm{M_O})_b$ centers. State R corresponds to both of these centers being in oxidized. State H_a and H_b correspond to the $(\mathrm{M-O})_a$ or $(\mathrm{M-O})_b$ center being reduced, respectively, while the other is oxidized. State $\mathrm{H}_a\mathrm{H}_b$ corresponds to both centers being reduced. The relative free energies of these four states are

given by

$$G_{\mathrm{H}_a\mathrm{H}_b} = 0 \quad , \tag{S14}$$

$$G_{\mathrm{H}_a} \quad = e(\eta_2 - \eta) \quad , \tag{S15}$$

$$G_{\mathrm{H}_b} \quad = e(\eta_1 - \eta) \quad , \tag{S16}$$

$$G_{\mathrm{R}} \quad = e(\eta_1 + \eta_2 - 2\eta) \quad . \tag{S17}$$

In writing the free energy expression for state H_a, we have assumed that the free energy to oxidize the $(\mathrm{M-O})_b$ center is the same regardless of whether the $(\mathrm{M-O})_a$ center is oxidized or reduced. Using these free energy expressions in eq (S13) for P_{R} and substituting into eq (S12) gives the rate expression in eq (1) of the main text,

$$\mathrm{TOF} = \frac{k_3}{\left[1 + \exp\left(-\frac{e(\eta - \eta_1)}{k_{\mathrm{B}}T}\right)\right]\left[1 + \exp\left(-\frac{e(\eta - \eta_2)}{k_{\mathrm{B}}T}\right)\right]} \quad . \tag{1}$$

Derivation of Equation (17)

The scaling relation used in ref S21 (eq (16) in the main text) expresses the formation free energy of the OOH intermediate on a given site in terms of the formation free energy of the OH intermediate (although these formation energies are called binding energies in ref S21),

$$\Delta G_{\mathrm{HOO}*} = \Delta G_{\mathrm{HO}*} + b' \quad . \tag{S18}$$

The formation free energies are defined as the free energy to form the intermediate from liquid water and bind it to an undercoordinated metal cation on the surface, with the protons and electrons removed in the process going to the reversible hydrogen electrode (RHE). Eq (16)

states that the formation free energies of the two intermediates are offset by a constant energy b'. This offset is equal to the free energy to form the OOH intermediate from the OH intermediate, which is equivalent to the sum of steps 1 and 3′ in the main text. Therefore, it is equal to

$$b' = e(\eta_1 + \eta_3 + 2.46\,\mathrm{V}) \quad , \tag{S19}$$

where the additional term $2U_{\mathrm{OER}}$ accounts for that fact that the RHE is used as the reference for the proton and electron free energies in ref S21, while the equilibrium potential of the OER (1.23 V vs. the RHE) is used in the present manuscript. Finally, making use of eqs (13) and (14) in the main text allows us to write b' in terms of the offset b of the scaling relation in (15),

$$b' = -b + e(\eta_{\mathrm{H}} + \eta_{\mathrm{H_2O}} + 2.46\,\mathrm{V}) \quad . \tag{17}$$

Activity Plot for the (110)-A Surface

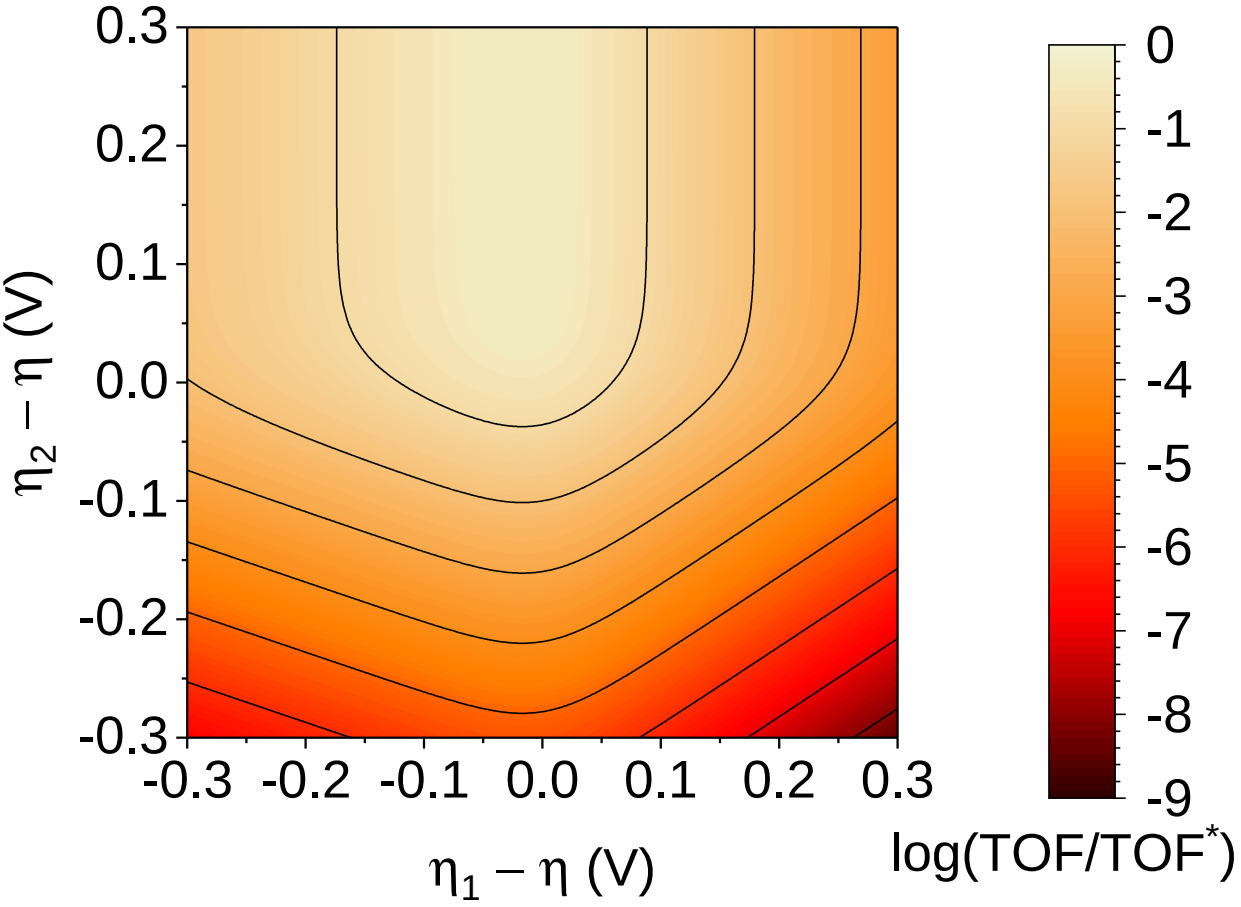

Figure S1

Structures of Surfaces Used in the Calculations

The three different surfaces examined herein were built from an optimized Co_3O_4 bulk crystal containing 8 formula units per unit cell and with an optimized lattice parameter of 8.16 Å. The surfaces were modeled as periodic slabs which were cut from the bulk and terminated in such a way that neutral surfaces were obtained with no net dipole moment normal to the surface. The periodic slabs were separated by a vacuum layer having a thickness of at least 7 Å. More details can be found in ref S4.

The doped active sites were created by replacing the two Co centers M_a and M_b (shown

in Figure 1 in the main text) with other 3d transition metals. For each surface and doping, four states of the active site were examined. These states are labeled H_aH_b, H_b, R, and P and are shown in Figures S2 – S4 for the three surfaces. In state H_aH_b both the $(M-O)_a$ and $(M-O)_b$ centers are in the reduced state, in state H_b the $(M-O)_a$ center is oxidized while the $(M-O)_b$ center is reduced, and in state R both centers are oxidized. State P is the product state of the water addition reaction. In addition to these states, a single transition state labeled TS was determined for the water addition step on the (311) and (110)-B surfaces. Two transition states were determined on the (110)-A surface, the first (TS-1) corresponding to the H^+/e^- transfer process and the second (TS-2) corresponding to the O–O bond formation process.

In all of the surface states examined, the Co cations in the surface outside of the active site were kept in fixed oxidation states, which are indicated in Figures S2 – S4 for the three surfaces. For some of the active sites on the (110)-A and (110)-B surfaces, it was not possible to converge these Co cations to the correct oxidation state in certain surface states. In these cases, either the Co^{4+} cations or all of the octahedrally coordinated Co cations in the surface were replaced by the less reducible of the dopant metals in the active site. These structures are labeled "M(IV)-all" and "M-all" in Tables S5 – S10, respectively.

On the (110)-A surface, two configurations were examined for each doping composition. In the first configuration, labeled "b", the more reducible metal is placed in the lower position on the active site. In the second configuration, labeled "t", the more reducible metal is placed in the upper position.

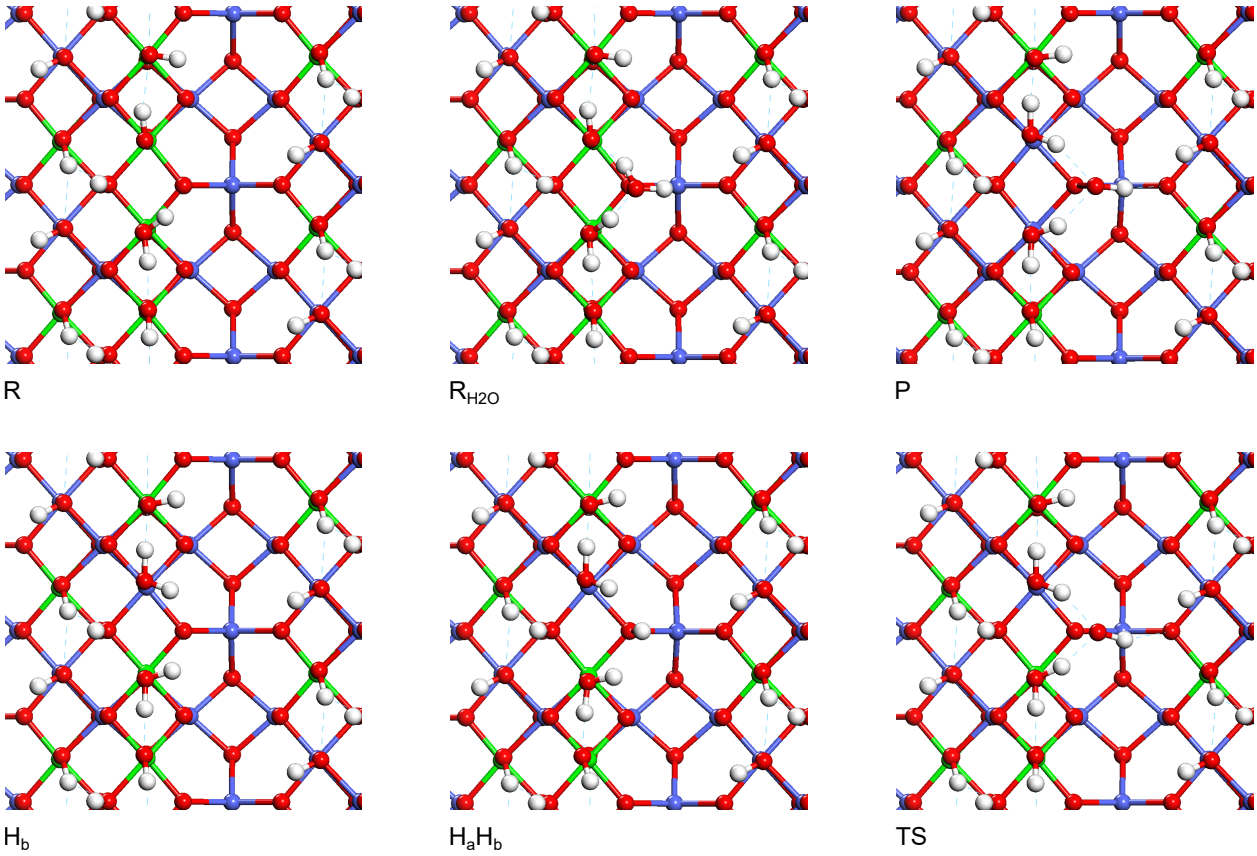

Figure S2: Structures of different states of the (311) surface. Oxidized metal centers in the +4 oxidation state are indicated in light green.

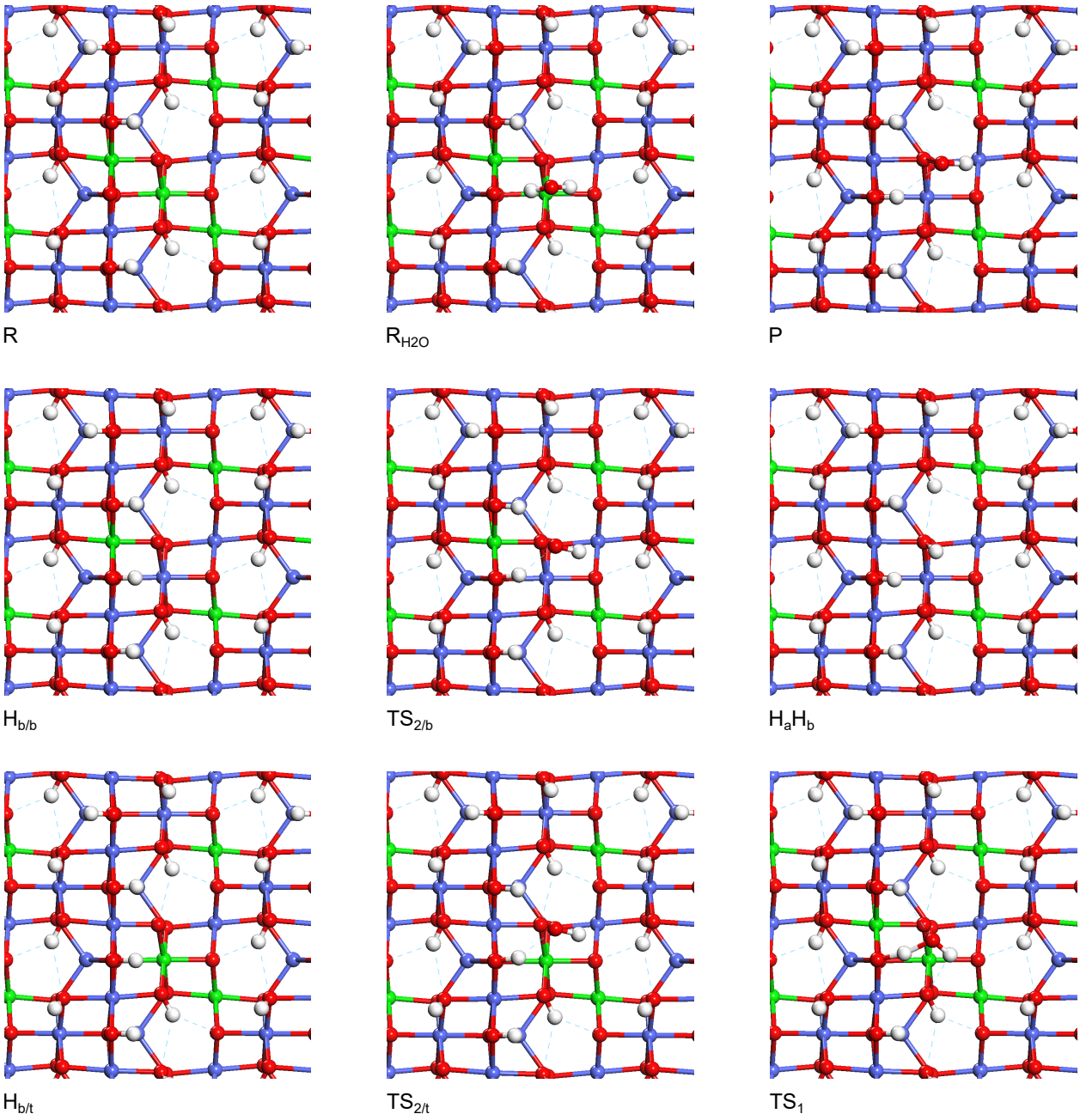

Figure S3: Structures of different states of the (110)-A surface. Oxidized metal centers in the +4 oxidation state are indicated in light green.

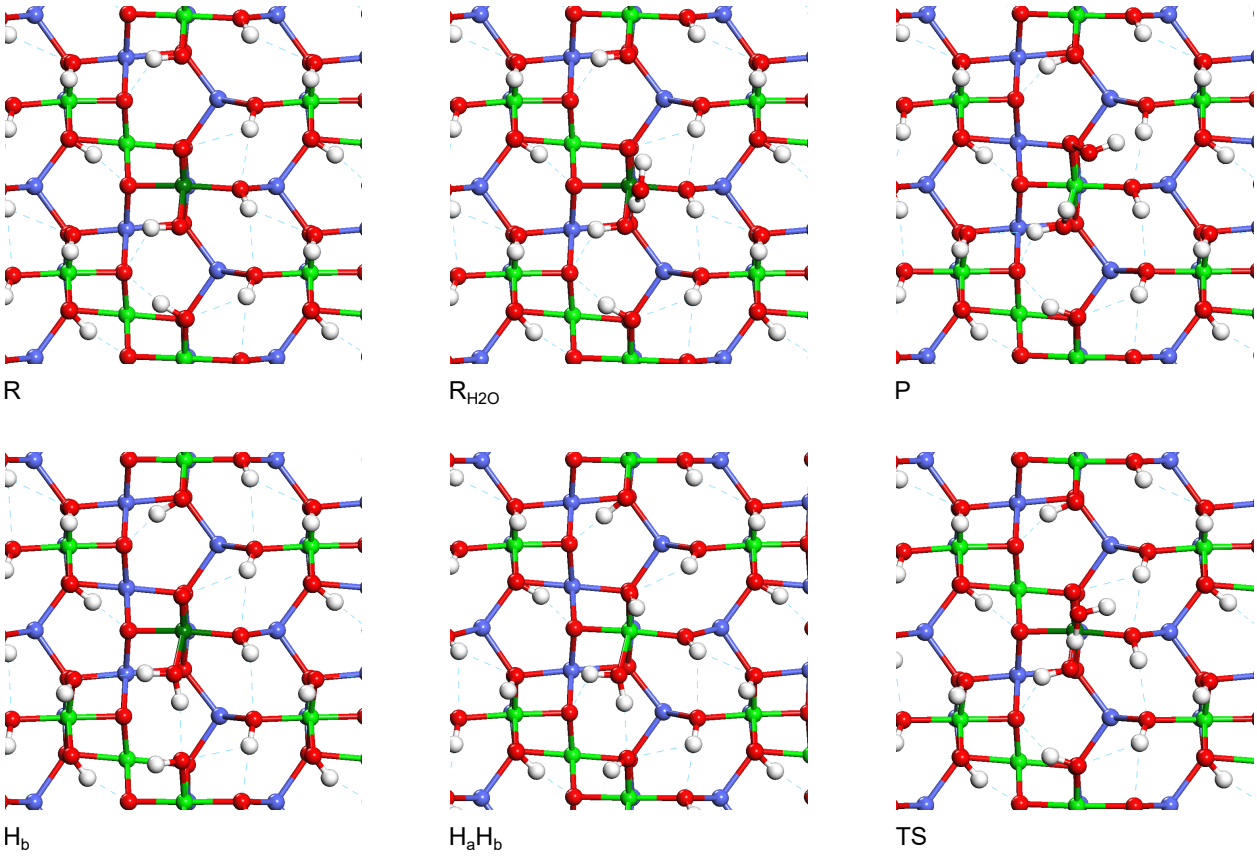

Figure S4: Structures of different states of the (110)-B surface. Oxidized metal centers are indicated in light green for the +4 oxidation state and dark green for the +5 oxidation state.

Tables of Selected Bond Distances

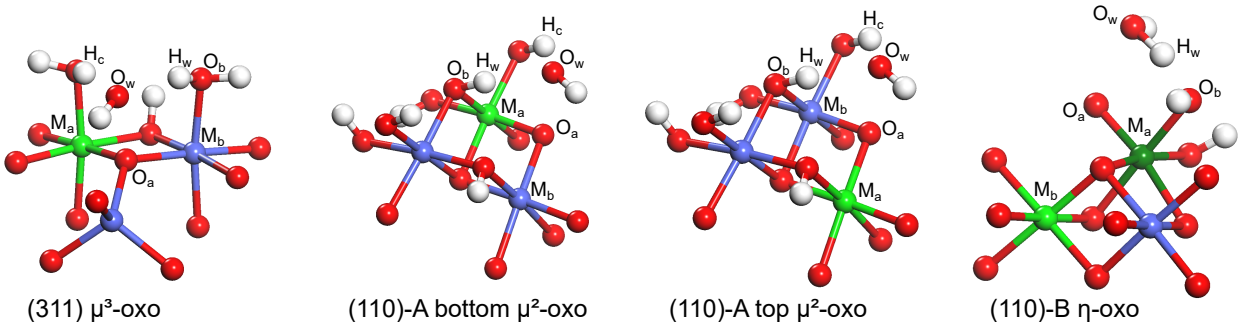

Figure S5: Labels for atom on each active site used to define the bond distances in the transition state for water addition listed in Tables S2 – S4

Table S2: Selected bond lengths (Å) in the transition states for sites on the (311) surface. Atom labels are defined in Figure S5.

M_a	M_b	O_a-O_w	O_w-H_w	O_b-H_w	O_w-H_c
V	V	1.820	1.928	0.987	2.117
V	Mn	1.803	1.945	0.985	2.203
V	Co	1.800	1.962	0.984	1.915
V	Cr	1.798	1.947	0.986	2.085
V	Ni	1.814	1.930	0.987	2.080
Mn	Mn	1.811	1.862	0.990	2.320
Mn	Co	1.823	1.888	0.989	1.920
Mn	Cr	1.807	1.856	0.991	2.099
Mn	Fe	1.804	1.845	0.991	2.221
Mn	Ni	1.855	1.703	1.007	2.280
Co	Co	2.057	1.687	1.004	1.819
Co	Cr	1.983	1.723	1.002	1.927
Co	Fe	1.961	1.842	0.992	1.878
Cr	Cr	2.140	1.719	1.004	1.891
Cr	Fe	1.917	1.871	0.990	1.978
Fe	Fe	1.931	1.905	0.989	2.013
Ni	Ni	2.015	1.715	1.004	1.974

Table S3: Selected bond lengths (Å) in the transition states for sites on the (110)-A surface. Atom labels are defined in Figure S5. See the section Structures of Surfaces Used in the Calculations for the meaning of "M(IV)-all", "t", and "b".

M_a	M_b		O_a-O_w	O_w-H_w	O_b-H_w	O_w-H_c
V	V	t	1.847	2.194	0.982	2.533
V	Mn	t	1.843	2.140	0.983	2.433
V	Fe	t	1.842	2.174	0.982	2.446
V	Cr	b	1.878	2.192	0.983	2.501
V	Cr	t	1.842	2.193	0.981	2.472
V	Co	b	1.896	2.151	0.983	2.465
Mn	Fe	t	2.058	2.160	0.985	2.272
Fe	Fe	b	2.083	2.191	0.985	2.196
Fe	Cr	b	2.110	2.080	0.989	2.296
Fe	Co	b	2.042	1.973	0.986	2.297
Co	Co	b	2.077	1.830	1.001	2.108
Co	Co	t	2.093	1.980	0.989	2.164
M(IV)-all						
V	Fe	b	1.870	2.280	0.982	2.441
V	Co	b	1.900	2.180	0.984	2.499
V	Co	t	1.863	2.130	0.983	2.230
Mn	Mn	b	1.921	2.340	0.985	2.459
Mn	Mn	t	2.054	2.083	0.987	2.415
Mn	Fe	b	1.857	2.220	0.986	2.272
Mn	Cr	b	1.908	2.060	0.991	2.362
Mn	Co	b	1.902	2.040	0.992	2.286

Table S4: Selected bond lengths (Å) in the transition states for sites on the (110)-B surface. Atom labels are defined in Figure S5. See the section Structures of Surfaces Used in the Calculations for the meaning of "M-all" and "M(IV)-all".

M_a	M_b	O_a-O_w	O_b-H_w	O_w-H_w
Cr	Co	2.077	1.103	1.372
Cr	Cr	2.001	1.077	1.431
Cr	Fe	1.961	1.060	1.467
Co	Co	2.052	1.384	1.100
M-all				
V	V	1.937	1.020	1.642
V	Mn	1.844	1.045	1.512
V	Fe	1.943	1.018	1.652
Cr	Co	2.094	1.125	1.334
Cr	Cr	2.022	1.079	1.421
Mn	V	1.850	1.078	1.428
Mn	Mn	1.869	1.082	1.412
Mn	Co	2.071	1.587	1.028
Mn	Cr	1.927	1.386	1.099
M(IV)-all				
V	V	1.954	1.022	1.628
V	Mn	1.788	1.017	1.649
Cr	Cr	2.022	1.079	1.421
Cr	Fe	1.943	1.046	1.510
Mn	V	1.826	1.059	1.465
Mn	Cr	1.944	1.379	1.102
Mn	Fe	1.913	1.339	1.123

Tables of Calculated Energies

Table S5: Calculated energies for sites on the (311) surface

M_a	M_b	η_1 V	η_2 V	ΔG_3 eV	$\Delta G_3^{\ddagger}$ eV	$\Delta G_{3'}$ eV	$\Delta G_{3'}^{\ddagger}$ eV
V	V	-0.51	-0.17	1.63	1.94	1.47	1.77
V	Mn	-0.50	0.15	1.37	1.71	1.52	1.86
V	Co	-0.54	0.53	0.92	1.24	1.45	1.76
V	Cr	-0.52	0.60	0.88	1.18	1.48	1.78
V	Ni	-0.47	0.72	0.71	1.07	1.43	1.79
Mn	Mn	-0.19	0.16	1.11	1.59	1.27	1.75
Mn	Co	-0.14	0.51	0.60	1.09	1.10	1.60
Mn	Cr	-0.16	0.53	0.66	1.17	1.19	1.70
Mn	Fe	-0.18	0.61	0.61	1.09	1.22	1.70
Mn	Ni	-0.14	0.72	0.44	0.99	1.15	1.70
Co	Co	0.21	0.49	0.16	0.81	0.65	1.30
Co	Cr	0.19	0.50	0.22	0.89	0.73	1.39
Co	Fe	0.01	0.55	0.35	0.97	0.90	1.51
Cr	Cr	0.34	0.57	0.05	0.71	0.62	1.28
Cr	Fe	-0.05	0.61	0.40	0.97	1.01	1.58
Fe	Fe	-0.07	0.68	0.34	0.93	1.02	1.61
Ni	Ni	0.41	0.69	-0.15	0.59	0.54	1.28

Table S6: Calculated energies for sites on the (110)-A surface. See the section Structures of Surfaces Used in the Calculations for the meaning of "M(IV)-all", "t", and "b".

M_a	M_b		η_1 V	η_2 V	ΔG_3 eV	$\Delta G_3^{\ddagger}$ eV	$\Delta G_{3'}$ eV	$\Delta G_{3'}^{\ddagger}$ eV
V	V	t	-0.35	-0.09	1.46	2.00	1.37	1.90
V	Mn	t	-0.33	0.52	0.74	1.29	1.26	1.80
V	Fe	t	-0.34	0.84	0.50	1.03	1.33	1.86
V	Cr	b	-0.08	0.60	0.53	1.22	1.13	1.82
V	Cr	t	-0.25	0.65	0.62	1.16	1.27	1.81
V	Co	b	-0.04	0.00			1.01	1.79
Mn	Fe	t	0.20	0.81	0.00	0.81	0.80	1.62
Co	Co	b	0.75	0.87	-0.70	0.51	0.18	1.38
Co	Co	t	0.82	0.81	-0.70	0.55	0.11	1.36
Fe	Fe	b	0.52	0.97	-0.50	0.67	0.47	1.64
Fe	Cr	b	0.69	0.75	-0.43	0.87	0.33	1.62
Fe	Co	b	0.69	0.82	-0.57	0.78	0.26	1.60
M(IV)-all								
V	Fe	b	0.00	0.66	0.56	1.18	1.21	1.83
V	Co	b	-0.05	0.00			1.03	1.79
V	Co	t	-0.358	0.85	0.49	0.98	1.34	1.83
Mn	Mn	b	0.121	0.53	0.26	1.20	0.79	1.73
Mn	Mn	t	0.23	0.42	0.26	1.16	0.68	1.58
Mn	Fe	b	0.016	0.00			0.94	1.69
Mn	Cr	b	0.199	0.00			0.76	1.64
Mn	Co	b	0.241	0.00			0.64	1.57

Table S7: Calculated energies for sites on the (110)-B surface. See the section Structures of Surfaces Used in the Calculations for the meaning of "M(IV)-all" and "M-all".

M_a	M_b	η_1 V	η_2 V	ΔG_3 eV	$\Delta G_3^{\ddagger}$ eV
Cr	Co	0.39	0.56	-0.22	1.26
Cr	Cr	0.38	0.69	-0.33	1.16
Cr	Fe	0.00	0.00	0.20	1.25
Co	Co	1.14	0.47	-0.78	0.73
M-all					
V	V	-0.16	-0.50	1.67	2.29
V	Mn	-0.11	-0.54	1.68	2.26
Cr	Co	0.43	0.43	0.15	1.40
Cr	Cr	0.27	0.68	0.06	1.20
Mn	Mn	1.24	-0.26	0.13	1.04
Mn	Co	1.05	0.84	-0.69	0.81
M(IV)-all					
V	V	-0.14	-0.38	1.56	2.24
V	Mn	-0.11	-0.46	1.65	2.19
Cr	Cr	0.45	0.70	0.03	1.11
Cr	Fe	0.44	0.46	0.22	1.15

Table S8: O−H and O−OH bond dissociation energies for sites on the (311) surface

M_a	M_b	ΔG_{O-H} eV	ΔG_{O-OH} eV
V	V	3.14	0.77
V	Mn	3.15	0.71
V	Co	3.12	0.78
V	Cr	3.14	0.75
V	Ni	3.18	0.80
Mn	Mn	3.47	0.96
Mn	Co	3.51	1.13
Mn	Cr	3.49	1.04
Mn	Fe	3.47	1.01
Mn	Ni	3.51	1.08
Co	Co	3.86	1.58
Co	Cr	3.84	1.51
Co	Fe	3.66	1.33
Cr	Cr	3.99	1.61
Cr	Fe	3.61	1.22
Fe	Fe	3.59	1.21
Ni	Ni	4.07	1.69

Table S9: O−H and O−OH bond dissociation energies for sites on the (110)-A surface. See the section Structures of Surfaces Used in the Calculations for the meaning of "M(IV)-all", "t", and "b".

M_a	M_b		ΔG_{O-H} eV	ΔG_{O-OH} eV
V	V	b	3.51	1.06
V	V	t	3.31	0.86
V	Mn	t	3.32	0.97
V	Fe	t	3.32	0.90
V	Cr	b	3.57	1.10
V	Cr	t	3.40	0.96
V	Co	b	3.61	1.22
Mn	Fe	b	3.76	1.39
Mn	Fe	t	3.86	1.43
Mn	Cr	b	3.91	1.51
Mn	Cr	t	4.03	1.59
Mn	Co	b	3.98	1.68
Mn	Co	t	3.90	1.51
Fe	Fe	b	4.17	1.76
Fe	Fe	t	4.23	1.82
Fe	Cr	b	4.34	1.91
Fe	Cr	t	4.32	1.85
Fe	Co	b	4.35	1.98
Fe	Co	t	4.24	1.79
Cr	Cr	b	4.41	1.95
Cr	Cr	t	4.40	1.94
Cr	Co	b	4.32	1.92
Cr	Co	t	4.23	1.81
Co	Co	b	4.41	2.06
Co	Co	t	4.47	2.12
M(IV)-all				
V	Mn	b	3.60	1.13
V	Co	b	3.60	1.20
V	Co	t	3.30	0.89
Mn	Mn	b	3.78	1.44
Mn	Mn	t	3.88	1.55
Mn	Fe	b	3.67	1.29
Mn	Cr	b	3.85	1.47
Mn	Co	b	3.90	1.59

Table S10: O−H and O−OH bond dissociation energies for sites on the (110)-B surface. See the section Structures of Surfaces Used in the Calculations for the meaning of "M(IV)-all" and "M-all".

M_a	M_b	ΔG_{O-H} eV	ΔG_{O-OH} eV
Cr	Co	4.05	1.89
Cr	Cr	4.04	1.88
Co	Co	4.80	2.54
M-all			
V	V	3.50	1.06
V	Mn	3.54	1.09
V	Co	3.60	0.86
V	Fe	3.47	1.02
Cr	Co	4.08	1.66
Cr	Cr	3.92	1.49
Mn	Mn	4.89	2.36
Mn	Co	4.71	2.08
M(IV)-all			
V	V	3.51	1.05
V	Mn	3.54	1.04
V	Fe	3.45	1.01
Cr	V	4.10	1.40
Cr	Cr	4.10	1.51
Cr	Fe	4.10	1.55

References

(S1) Kresse, G.; Furthmüller, J. Efficient iterative schemes for ab initio total-energy calculations using a plane-wave basis set. *Phys. Rev. B* **1996**, *54*, 11169–11186.

(S2) Hammer, B.; Hansen, L. B.; Nørskov, J. K. Improved adsorption energetics within density-functional theory using revised Perdew-Burke-Ernzerhof functionals. *Phys. Rev. B* **1999**, *59*, 7413–7421.

(S3) Cohen, A. J.; Mori-Sanchez, P.; Yang, W. Insights into current limitations of density functional theory. *Science (80-.).* **2008**, *321*, 792–794.

(S4) Plaisance, C. P.; van Santen, R. A. Structure sensitivity of the oxygen evolution reaction catalyzed by cobalt(II,III) oxide. *J. Am. Chem. Soc.* **2015**, *137*, 14660–14672.

(S5) Plaisance, C. P.; Reuter, K.; van Santen, R. A. Quantum chemistry of the oxygen evolution reaction on cobalt(II,III) oxide - Implications for designing the optimal catalyst. *Faraday Discuss.* **2016**, *188*, 199–226.

(S6) Anisimov, V. I.; Gunnarsson, O. Density-functional calculation of effective Coulomb interactions in metals. *Phys. Rev. B* **1991**, *43*, 7570–7574.

(S7) Liechtenstein, A. I. I.; Anisimov, V. I.; Zaanen, J. Density-functional theory and strong interactions: Orbital ordering in Mott-Hubbard insulators. *Phys. Rev. B* **1995**, *52*, R5467–R5470.

(S8) Anisimov, V. I.; Aryasetiawan, F.; Lichtenstein, A. I. First-principles calculations of the electronic structure and spectra of strongly correlated systems: the LDA + U method. *J. Phys. Condens. Matter* **1997**, *9*, 767–808.

(S9) Plaisance, C. P.; van Santen, R. A.; Reuter, K. Constrained-orbital density functional theory. Computational method and applications to surface chemical processes. *J. Chem. Theory Comput.* **2017**, 3561–3574.

(S10) Henkelman, G.; Uberuaga, B. P.; Jonsson, H. A climbing image nudged elastic band method for finding saddle points and minimum energy paths. *J. Chem. Phys.* **2000**, *113*, 9901.

(S11) Henkelman, G.; Jonsson, H. Improved tangent estimate in the nudged elastic band method for finding minimum energy paths and saddle points. *J. Chem. Phys.* **2000**, *113*, 9978.

(S12) Henkelman, G.; Jonsson, H. A dimer method for finding saddle points on high di-

mensional potential surfaces using only first derivatives. *J. Chem. Phys.* **1999**, *111*, 7010.

(S13) Bearpark, M. J.; Robb, M. A.; Bernhard Schlegel, H. A direct method for the location of the lowest energy point on a potential surface crossing. *Chem. Phys. Lett.* **1994**, *223*, 269–274.

(S14) Allen, J. P.; Watson, G. W. Occupation matrix control of d- and f-electron localisations using DFT + U. *Phys. Chem. Chem. Phys.* **2014**, *16*, 21016–21031.

(S15) Bengone, O.; Alouani, M.; Blöchl, P.; Hugel, J. Implementation of the projector augmented-wave LDA+ U method: Application to the electronic structure of NiO. *Phys. Rev. B* **2000**, *62*, 392–401.

(S16) Sit, P. H.; Car, R.; Cohen, M. H.; Selloni, A. Simple, unambiguous theoretical approach to oxidation state determination via first-principles calculations. **2011**, 10259–10267.

(S17) Qian, X.; Li, J.; Qi, L.; Wang, C.-Z.; Chan, T.-L.; Yao, Y.-X.; Ho, K.-M.; Yip, S. Quasiatomic orbitals for ab initio tight-binding analysis. *Phys. Rev. B* **2008**, *78*, 245112.

(S18) Nørskov, J. K.; Rossmeisl, J.; Logadottir, A.; Lindqvist, L.; Kitchin, J. R.; Bligaard, T.; Jónsson, H. Origin of the overpotential for oxygen reduction at a fuel-cell cathode. *J. Phys. Chem. B* **2004**, *108*, 17886–17892.

(S19) Rossmeisl, J.; Qu, Z.-W.; Zhu, H.; Kroes, G.-J.; Nørskov, J. Electrolysis of water on oxide surfaces. *J. Electroanal. Chem.* **2007**, *607*, 83–89.

(S20) Wang, L.; Maxisch, T.; Ceder, G. Oxidation energies of transition metal oxides within the GGA+U framework. *Phys. Rev. B* **2006**, *73*, 195107.

(S21) Man, I. C.; Su, H.-Y.; Calle-Vallejo, F.; Hansen, H. A.; Martínez, J. I.; Inoglu, N. G.; Kitchin, J.; Jaramillo, T. F.; Nørskov, J. K.; Rossmeisl, J. Universality in oxygen evolution electrocatalysis on oxide surfaces. *ChemCatChem* **2011**, *3*, 1159–1165.